Mater. Res. Soc. Symp. Proc. Vol. 1490 © 2013 Materials Research Society
DOI: 10.1557/opl.2013.85

High-temperature thermoelectric properties of W-substituted $CaMnO_3$

Dimas S. Alfaruq [a], James Eilertsen [a], Philipp Thiel [a], Myriam H Aguirre [a], Eugenio Otal [a], Sascha Populoh [a], Songhak Yoon [a], Anke Weidenkaff [a,*]
[a] *Empa, Solid State Chemistry and Catalysis, Ueberlandstrasse. 129, CH-8600 Duebendorf, Switzerland*
[*] *Corresponding Author*

Abstract

The thermoelectric properties of W-substituted $CaMn_{1-x}W_xO_{3-\delta}$ (x = 0.01, 0.03; 0.05) samples, prepared by soft chemistry, were investigated from 300 K to 1000 K and compared to Nb-substituted $CaMn_{0.98}Nb_{0.02}O_{3-\delta}$. All compositions exhibit both an increase in absolute Seebeck coefficient and electrical resistivity with temperature. Moreover, compared to the Nb-substituted sample, the thermal conductivity of the W-substituted samples was strongly reduced. This reduction is attributed to the nearly two times greater mass of tungsten. Consequently, a ZT of 0.19 was found in $CaMn_{0.97}W_{0.03}O_{3-\delta}$ at 1000 K, which was larger than ZT exhibited by the 2% Nb-doped sample.

1. Introduction

Thermoelectric materials convert heat into electricity directly. Their thermoelectric efficiency is nominally quantified by a dimensionless figure of merit (ZT). The ZT is a function of the interdependent electrical and thermal transport properties of the material; specifically, the Seebeck coefficient (S), electrical resistivity (ρ), and total thermal conductivity (κ) – determined at a particular temperature (T) in Kelvin: $ZT = S^2T/\rho\kappa$, where $\kappa = \kappa_l + \kappa_e$.

Consequently, in order to enhance the ZT of a thermoelectric material, a high Seebeck coefficient must be maintained while the electrical resistivity and the total thermal conductivity of the material are reduced[1]. This can be achieved, in part, by introducing additional charge carriers up to a suitable concentration. As a result, the electrical resistivity can be reduced without reducing the Seebeck coefficient appreciably. Aliovalent transition-metal cation substitution, in particular with comparatively heavy transition metals, can achieve both increased charge carrier concentration and decreased lattice thermal conductivity due to mass-difference phonon scattering [1-3].

The calcium manganate, $CaMnO_3$, is a promising thermoelectric material as it exhibits high Seebeck coefficients, strong resistance to chemical degradation at elevated temperatures, and a perovskite-type structure susceptible to A- and B-site substitution [4]. Therefore, this paper reports an investigation into the effect of aliovalent B-site substitution on the structure and thermoelectric properties of $CaMnO_3$. W-substituted $CaMn_{1-x}W_xO_{3\pm\delta}$ (x = 0.01; 0.03; 0.05) samples were prepared by soft chemistry, sintered, and characterized by x-ray diffraction and electron microscopy. Thermogravimetric analysis experiments were performed to determine the oxygen stoichiometry of each sample. The thermoelectric properties were measured from 300 K to 1000 K and compared to Nb-substituted $CaMn_{0.98}Nb_{0.02}O_{3-\delta}$ [4] in order to evaluate the effectiveness of W-substitution.

2. Experimental

Polycrystalline perovskite-type $CaMn_{1-x}W_xO_{3\pm\delta}$ (x = 0.01; 0.03; 0.05) samples were synthesized via a procedure developed by Bocher et al.[4]. The samples were prepared by dissolving stoichiometric amounts of $Ca(NO_3)_2{\cdot}4H_2O$ (Fluka, ≥99.0%), $Mn(NO_3)_2{\cdot}4H_2O$ (Merck, 98%), and citric acid (Alfa Aesar, +98%) in distilled water. The WCl_6 (Aldrich, 99.0%) was

dissolved in isopropanol and added to the citric acid solution. The citric acid to total cation (Ca, Mn, W) ratio was 2:1. The solution was polymerized at 353 - 363 K for 4 hours under continuous stirring. The polymerized product was heated at 353 K for 16 hours to obtain the xerogel precursor. The xerogel precursor was heated to 573 K at a rate of 20 K/min to eliminate organic material; then crushed, ground in a mortar and pestle, heated at a rate of 5 K/min to 1373 K, and calcined for 8 hours. The Nb-substituted $CaMn_{0.98}Nb_{0.02}O_{3\pm\delta}$ sample was synthesized as above. The samples were pressed uniaxially using a hydrostatic press, heated at a rate of 5 K/min to 1473 K, sintered for 5 h, and cooled at a rate of 5 K/min.

Powder X-ray diffraction (PXRD) patterns were obtained using a PANalytical X´Pert PRO θ-2θ scan system equipped with Johansson monochromator and the ultra-fast X'Celerator linear detector. The incident X-rays had a wavelength of 0.154056 nm (Cu-$K\alpha_1$). The diffraction patterns were scanned from 20˚ to 100˚ (2θ) with an angular step interval of 0.0167˚. PXRD data was analyzed with the Le Bail technique by using the Fullprof Suite software package [5,6], and Thompson-Cox-Hastings pseudo-Voigt profile fitting functions. High-resolution transmission electron microscopy (HRTEM) and electron diffraction (ED) studies were carried out using a Jeol JEM FS2200 electron microscope.

The oxygen stoichiometry was determined by reducing the sintered samples and measuring their mass loss using a Netzsch STA 409 CD thermogravimetric analysis (TGA). The samples were heated at a rate of 20 K/min to 1373 K under a reducing atmosphere (20% vol H_2/He). The atmosphere reduced the $CaMn_{1-x}W_xO_{3\pm\delta}$ phase and generated an evolution of H_2O vapor and the formation of MnO and CaO:

$$CaMn_{1-x}W_xO_3(s) + H_2 \xrightarrow{1373\,K} CaO(s) + (1-x)MnO(s) + (x)W(s) + H_2O\ (g) \quad \text{(eq.2)}$$

Thermoelectric data were collected from 300 K to 1000 K in synthetic air on samples sintered to approximately 85% of their theoretical density. Seebeck coefficient (S) and electrical resistivity (ρ) data were collected on rectangular-shaped samples by using an RZ2001i unit from Ozawa Science (Japan). Thermal diffusivities were measured using a Netzsch LFA 457 laser flash apparatus. A Netzsch DSC 404 C Pegasus with sapphire standard was used to measure the heat capacity (C_p) of the compounds by the ratio method. Thermal conductivity (κ) was determined from thermal diffusivity (α) and heat capacity (C_p) data, and the sample density (d) according to the relationship: $\kappa = \alpha * d * C_p$.

3. Results and Discussions

PXRD data and the Le Bail profile fit of the $CaMn_{0.99}W_{0.01}O_{3-\delta}$ sample are shown (Fig. 1a). All samples crystallized into the perovskite-type orthorhombic crystal structure with *Pnma* space group. A systematic increase in the unit cell volume is observed with tungsten substitution (Fig.1b). The unit cell volume data[7] for $CaMnO_3$ is included in the figure. The tungsten-substituted samples do not deviate from linearity appreciably. Note the perovskite-type crystal structure depicted in the inset.

Twin domains were observed by using HRTEM (Fig. 2). The Fast Fourier Transformed (simulated by Digital Micrograph 3.8.2 Gatan software) taken from different regions of the HRTEM image indicates the superposition of the two zone-axis ([10-1] and [101]), these are identical in the orthorhombic structure and form twin domains. These domains are typically between 30 and 50 nm. The twin domains likely occur because the $CaMnO_3$ compound undergoes a structural transition from a higher symmetry, cubic structure (the high-temperature structure), to a lower symmetry, orthorhombic structure (the low-temperature structure). Since the deviations from the cubic symmetry are small and the orthorhombic structure of $CaMnO_3$ can be described with $\sqrt{2}a \times 2a \times \sqrt{2}a$ unit cell, domains with different

unit-cell orientations can grow coherently, thus yielding the observed twinning phenomenon[8,9].

Oxygen deficiencies of δ=0.039, 0.112, and 0.179 for the respective x = 0.01, 0.03, and 0.05 $CaMn_{1-x}W_xO_{3-\delta}$ samples were determined by TGA. A systematic increase in oxygen deficiency occurs with increasing tungsten concentration.

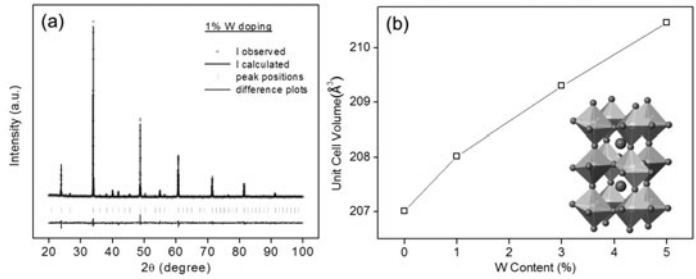

Figure 1: PXRD data and Le Bail profile fit of $CaMn_{0.99}W_{0.01}O_{3\pm\delta}$ (a). The unit cell volume expansion with increasing tungsten concentration (b). The crystal structure of the calcium manganate perovskite is shown (inset): the red spheres represent calcium, the blue represent oxygen, and the manganese and tungsten are located at the center of the octahedra.

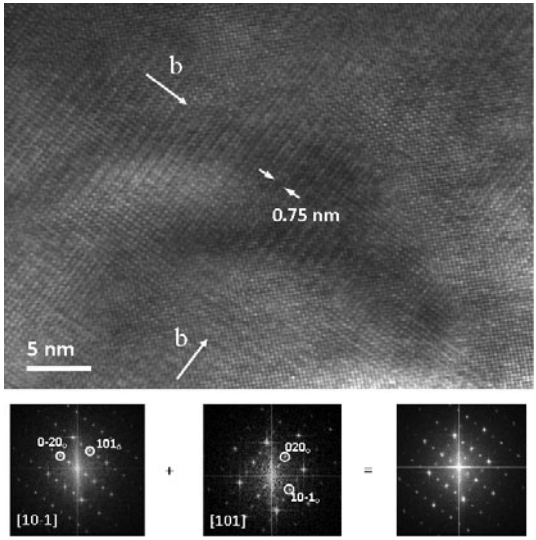

Figure 2: HRTEM of $CaMn_{1-x}W_xO_3$ showing a twin domain structure (the [10-1] and [101] zone axis).

The electrical resistivity data is shown (Fig. 3a). The electrical resistivity of all samples increases with increasing temperature, a trend consistent with heavily doped semiconductors. Moreover, the electrical resistivity drops with increasing tungsten concentration. The resistivity of the 2% Nb-substituted sample is higher than all of the W-substituted samples over the majority of the temperature range measured. Aliovalent substitutions of both W^{6+} and Nb^{5+} for Mn^{4+} likely induce mixed valence cations; namely, Mn^{3+} and Mn^{4+}. Electrons can hop from the Mn^{3+} to Mn^{4+}, mediated by the 2p electrons in oxygen, thus decreasing the electrical resistivity[10]. Therefore, tungsten will supply more charge carriers than an equivalent amount of niobium, providing a possible explanation for the comparatively lower electrical resistivity in the W-substituted samples [11]. The electrical resistivity of the 1% W- and 2% Nb-substituted samples, however, are quite similar. Since tungsten and niobium likely possess hexavalent and pentavalent oxidation states, respectively, the concentration of Mn^{3+} in both compositions is likely to be similar – leading to similar electrical resistivity in both.

The Seebeck (S) coefficient data is shown (Fig. 3b). Sizable negative Seebeck coefficients are observed in all samples. The magnitude of the Seebeck coefficients increased with increasing temperature consistent with the concomitant rise in electrical resistivity. Moreover, the magnitude of the Seebeck coeffcients tended to drop with increasing tungsten substitution as the charge carrier concentration increases (and the electrical resistivity decreases) with substitution [1,12,13].

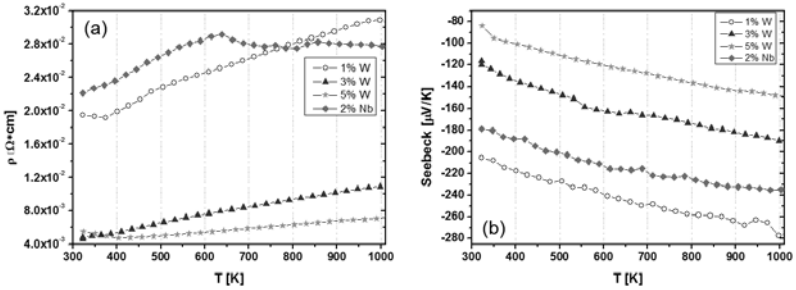

Figure 3: Temperature dependent resistivity (a) and Seebeck coefficient (b) data of the W-substituted $CaMn_{1-x}W_xO_3$ (x = 0.01; 0.03; 0.05) and 2% Nb-substituted samples.

The total thermal conductivity and lattice thermal conductivity data of the W-substituted $CaMn_{1-x}W_xO_{3\pm\delta}$ (x = 0.01; 0.03; 0.05) and 2% Nb-substituted $CaMn_{0.98}Nb_{0.02}O_{3\pm\delta}$ samples are shown (Fig. 4a, b). The lattice thermal conductivity is calculated by subtracting the electronic component from the total thermal conductivity. The electronic component was calculated from the electrical resistivity data using the Wiedemann-Franz law: $\kappa_e = L_oT/\rho$, where L_o was taken as the Sommerfeld value of the Lorenz constant (2.443×10^{-8} WΩ/K), and ρ is the electrical resistivity of the material. The total thermal conductivity is dominated by the lattice component as observed in other substituted calcium manganates[3,4,13,14]. The total and lattice thermal conductivity of the 2% Nb-substituted sample is higher than all of the W-substituted samples. For example, at 1000 K the lattice thermal conductivity of the 2% Nb-substituted sample reached 2.16 W/mK while all of the W-substituted samples, including the 1% W-substituted sample, are less than 1.8 W/mK at the same temperature. Since the atomic mass of tungsten is nearly two times that of niobium, and more than three times the mass of manganese, tungsten substitution enhances the mass-difference phonon scattering in the crystal structure significantly. Moreover, at lower tem-

peratures, the lattice thermal conductivity is reduced more significantly as mass-difference phonon scattering is more effective in this temperature range.

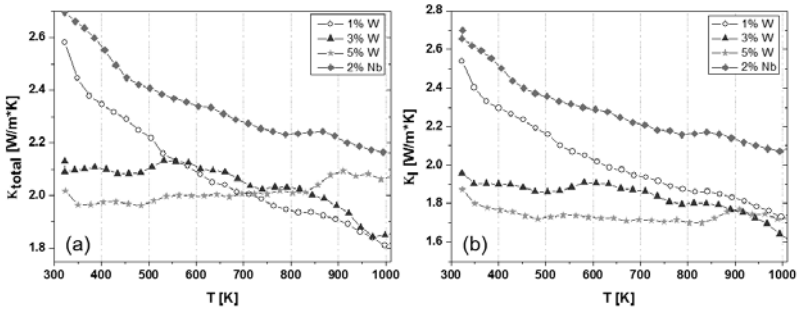

Figure 4: (a) Total thermal conductivity (κ_{total}) of $CaMn_{1-x}W_xO_3$ (x= 0.01; 0.03; 0.05) and $CaMn_{0.98}Nb_{0.02}O_{3\pm\delta}$; (b) Electronic thermal conductivity (κ_{el}) of $CaMn_{1-x}W_xO_3$ (x= 0.01; 0.03; 0.05); (c) Phonon thermal conductivity (κ_{ph}) of $CaMn_{1-x}W_xO_3$ (x= 0.01; 0.03; 0.05)

The ZT of the $CaMn_{1-x}W_xO_{3\pm\delta}$ (x = 0.01; 0.03; 0.05) and 2% Nb-substituted $CaMn_{0.98}Nb_{0.02}O_{3\pm\delta}$ sample was calculated for the 300 K to 1000 K temperature range. The 3% W-substituted $CaMn_{0.97}W_{0.03}O_{3\pm\delta}$ sample exhibits the highest ZT of the W-substituted samples, nearly reaching 0.2 at 1000 K. The low electrical resistivity and thermal conductivity achieved by tungsten substitution enhances the ZT significantly. However, the ZT of 2% Nb-substituted nanostructured samples reached 0.32 at 1060 K[4].

4. Conclusion

Polycrystalline W-substituted $CaMn_{1-x}W_xO_{3\pm\delta}$ (x = 0.01; 0.03; 0.05) samples were synthesized by a soft chemistry method. All samples crystallized into an orthorhombic crystal structure with *Pnma* space group. It was found that there was a systematic decrease in oxygen content with increasing tungsten concentration. The Seebeck coefficient, electrical resistivity, and thermal conductivity data were measured at elevated temperatures. The Seebeck coefficient and electrical resistivity is reduced with increasing tungsten substitution. The lowest electrical resistivity was achieved by the $CaMn_{0.95}W_{0.05}O_{3\pm\delta}$ sample while the $CaMn_{0.99}W_{0.01}O_{3\pm\delta}$ sample exhibits the highest Seebeck coefficient value at 1000 K (-270 μV/K). The thermal conductivity of all of the W-substituted samples is reduced in comparison to the 2% Nb-substituted sample due to enhanced mass-difference phonon scattering. Due to the interdependence of the Seebeck coefficient and the electrical resistivity, the best thermoelectric performance of the tungsten-substituted samples was obtained in the 3% W-substituted $CaMn_{0.97}W_{0.03}O_{3\pm\delta}$ sample with a ZT of 0.19 at 1000 K. The ZT was found to be lower than the 2% Nb-substituted sample, however, which reached a ZT of 0.32 at 1060 K[4]. Nevertheless, tungsten substitution is more effective than niobium substitution at reducing the thermal conductivity of the calcium manganates.

Acknowledgements

The authors would like to thank the Swiss Federal Office of Energy (BfE), Sinergia TEO (SNF) and Empa for the financial support.

References

(1) Rowe, D. M. *Thermoelectrics Handbook - Macro to Nano*; CRC Press/Taylor & Francis Group: Boca Raton, 2006.

(2) Funahashi, R.; Kosuga, A.; Miyasou, N.; Takeuchi, E.; Urata, S.; Lee, K.; Ohta, H.; Koumoto, K. *Appl. Phys. Lett* **2007**, p 124.

(3) Wang, Y.; Sui, Y.; Wang, X.; Su, W.; Liu, X.; Fan, H. J. *Acta Mater.* **2010**, *58*, 6306.

(4) Bocher, L.; Aguirre, M. H.; Logvinovich, D.; Shkabko, A.; Robert, R.; Trottmann, M.; Weidenkaff, A. *Inorg. Chem.* **2008**, *47*, 8077.

(5) Lebail, A.; Duroy, H.; Fourquet, J. L. *Mater. Res. Bull.* **1988**, *23*.

(6) Rodriguez-Carvajal, J. *Physica B* **1993**, *192*, 55.

(7) Poeppelmeier, K. R.; Leonowicz, M. E.; Scanlon, J. C.; Longo, J. M.; Yelon, W. B. *Journal of Solid State Chem.* **1982**, *45*.

(8) Aguirre, M. H.; Canulescu, S.; Robert, R.; Homazava, N.; Logvinovich, D.; Bocher, L.; Lippert, T.; Dobeli, M.; Weidenkaff, A. *J. Appl. Phys.* **2008**, *103*, 013703.

(9) M.H. Aguirre, D. L., L. Bocher, R. Robert, S.G. Ebbinghaus and A. Weidenkaff *Acta Mater.* **2008** *57*, 108.

(10) Zener, C. *Phys. Rev.* **1951**, *82*, 403.

(11) Raveau, B.; Zhao, Y. M.; Martin, C.; Hervieu, M.; Maignan, A. *J. Solid State Chem.* **2000**, *149*, 203.

(12) Horiguchi, K. I.; Teduka, Y.; Sugihara, S. *Funtai Oyobi Fummatsu Yakin/ J. Japan Soc. of Powder and Powder Metall.* **2007**, *54*, 351.

(13) Wang, Y.; Sui, Y.; Fan, H.; Wang, X.; Su, Y.; Su, W.; Liu, X. *Chem.Mater.* **2009**, *21*, 4653.

(14) Maignan, A.; Martin, C.; Autret, C.; Hervieu, M.; Raveau, B.; Hejtmanek, J. *J. Mater. Chem.* **2002**, *12*, 1806.